†**Electronic Supplementary Information**

3D Nanostructured Inkjet Printed Graphene via UV-Pulsed laser Irradiation Enables Paper-Based Electronics and Electrochemical Devices

Suprem R. Das[1,3,#], Qiong Nian[2,4,#], Allison A. Cargill[1], John A. Hondred[1,3], Shaowei Ding[1], Mojib Saei[2], Gary J. Cheng[2,4,], Jonathan C. Claussen[1,3,*]*

[1]Department of Mechanical Engineering, Iowa State University, Ames, Iowa 50011

[2]School of Industrial Engineering, Purdue University, West Lafayette, Indiana 47907

[3]Division of Materials Science and Engineering, Ames Laboratory (DOE), Ames, Iowa 50011

[4]Birck Nanotechnology Center, Purdue University, West Lafayette, Indiana 47907

[#]these authors contributed equally to this work

* Corresponding authors' Email: jcclauss@iastate.edu ; gjcheng@purdue.edu

This supplementary information contains:

1. Supplementary Text
2. Supplemental Figures & Tables
3. References

1. Supplemental Text

Molecular Dynamics Simulation

The standard velocity-Verlet integrator is used to update the position of atoms based on Newton's equations of motion:

$$M\ddot{x}(t) = F(x(t))$$

where $x(t)$ and $\ddot{x}(t)$ are the position and the acceleration vector of each atom, M denotes the mass of atom, and F is the net force calculated from atomic interactions. The position of atoms is updated through the following time stepping method:

$$x_k(t + \Delta t) = x_k(t) + v_k(t)\Delta t + {}^{1}\!/_{2}\, a_k(t)\Delta t^2$$

where Δt, *v*, and *a* are associated with the timestep, velocity, and acceleration of the atom at current time (*t*) respectively. This formula evaluates the updated position for all 3 directions (*i.e.*, k = 1, 2, 3) at time $t + \Delta t$. Velocity is calculated and updated with the following equations:

$$v_k(t) = v_k\left(t - {}^{\Delta t}\!/_{2}\right) + {}^{1}\!/_{2}\, a_k(t)\Delta t$$

$$v_k\left(t - {}^{\Delta t}\!/_{2}\right) = v_k(t) + {}^{1}\!/_{2}\, a_k(t - \Delta t)\Delta t$$

Evaluation of acceleration for each time step is performed through the following equation:

$$a_k(t) = {}^{1}\!/_{m} F_k(x(t))$$

Force is measured as the derivative of potential designated between atoms. For example, this can be accomplished with through the use of the Lennard-Jones potential:

$$V_{ij} = 4\varepsilon\left[\left(\frac{\sigma_{ij}}{r_{ij}}\right)^{12} - \left(\frac{\sigma_{ij}}{r_{ij}}\right)^{6}\right]$$

Therefore, the applied force from atom *i* on atom *j* is equal to:

$$F_{ij} = 4\varepsilon \left[12\left(\frac{\sigma_{ij}}{r_{ij}}\right)^{11} - 6\left(\frac{\sigma_{ij}}{r_{ij}}\right)^{5}\right]$$

Where ε is the depth of the potential well, σ is the equilibrium distance for zero potential, and *r* is the distance between atoms.

Periodic boundary conditions are set in all 3 directions to maintain the number of atoms constant and the volume of the simulation cell fixed. These periodic boundary conditions permit cohesion between elements so that atoms exiting one boundary will result in atoms entering from the opposite face. The model designed with periodic boundaries will permit atomic interactions as well as interactions between graphene flakes as would be expected in a real-world scenario. In the current work a separate atom type is attributed to each graphene flake to help with the visualization as well as setup of the Lennard-Jones potential for inter-layer interactions. In the equilibrium state, the canonical ensemble is used to reach a stationary temperature of 300 K. NVT ensemble (*i.e.*, the canonical ensemble where the amount of substance (N), volume (V), and temperature (T) are conserved) is favored over NPT (where the isothermal–isobaric ensemble, amount of substance (N), pressure (P) and temperature (T) are conserved) due to the large free space in the simulation box. In this scenario, the barostat from the NPT ensemble will force the simulation box to shrink—a result that is not realistic for the case of floating graphene flakes. However in an NVT ensemble, the number of atoms as well as the volume and temperature of the simulation box will be held constant. To obtain the target temperature a Noose-hoover thermostat is implemented via the NVT ensemble. This Noose-hoover thermostat affects the velocity of atoms by:

$$\frac{d\vec{v}(t)}{dt} = \frac{F(t)}{m} - \zeta \vec{v}(t)$$

ζ is thermodynamic friction coefficient given by the following equation:

$$\frac{d\zeta(t)}{dt} = \frac{1}{M_s}[\sum_{i=1}^{N}\frac{1}{2}m(\vec{v(t)})^2 + (X+1)k_B T]$$

where M_s is the thermal inertia parameter (i.e., the energy constant multiplied by time constant to the power of two), *N* is the total number of atoms, and *X* is the degree of freedom corresponding to the system (3N), k_B is boltzmann constant and *T* is temperature of system in units of kelvin, which can be calculated by:

$$T = \frac{2E_{kin}}{3Nk_B} = \frac{1}{3Nk_B}\sum_{i=1}^{N}\frac{1}{2}m(\vec{v(t)})^2$$

In this formula E_{kin} is the indicator of total kinetic energy of the system.

The time constant for the Nose-hoover thermostat is set to 100 timesteps (0.1ps) which forces the simulation to reach a regulated temperature of 300 K in 0.1ps. However, the laser heating is performed by a NVE ensemble, where a heating source of 500 eV/ps per graphene flake is applied. This heating is simulated by scaling the velocity of atoms which will result in temperature rise as denoted in the last equation. The OVITO package is used for visualization [S5].

2. Supplemental Figures & Tables

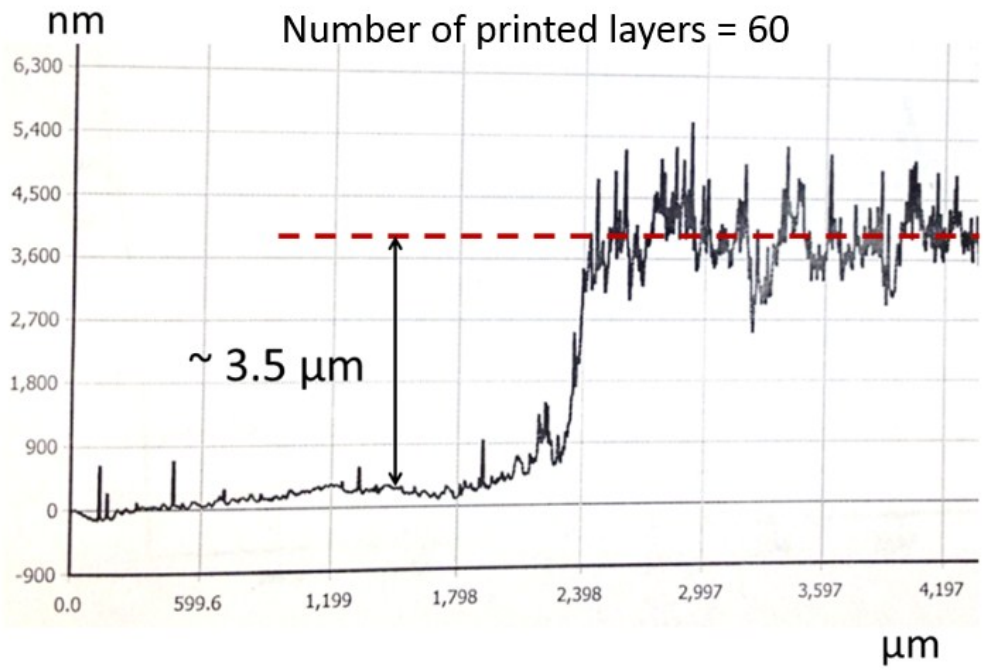

Figure S1: Profliometer thickness measurement of a graphene electrode inkjet printed on a polyimide substrate. The graphene electrode was created with 60 printer passes and was subsequently laser annealed with a power density of 85 mJ cm^{-2}. The thickness measurement is noticeably rough—a characteristic that is consistent with the development of petal-like graphene petals (see FESEM images of the graphene electrodes annealed with a laser power density of 85 mJ cm^{-2}: Fig. S4).

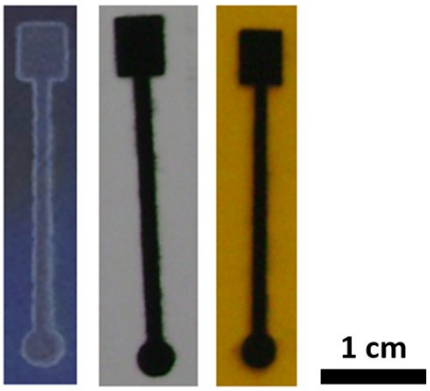

Figure S2: From Left to Right: (left) snapshots of graphene inkjet printed on n^{++}-Si/SiO_2 (300 nm) wafer, (middle) Kodak® cellulose photo paper, and (right) Kapton® polyimide foil. All substrates (except cellulose paper, which was simply dried with a nitrogen gun) were cleaned with acetone and methanol and subsequently dried with nitrogen gas prior to printing. Initial inkjet printing tests were performed on silicon to verify the printer settings and ink viscosity requirements necessary for inkjet printing graphene. The experiments performed in this work were conducted with graphene inkjet printed on flexible substrates, viz., cellulose and polymide.

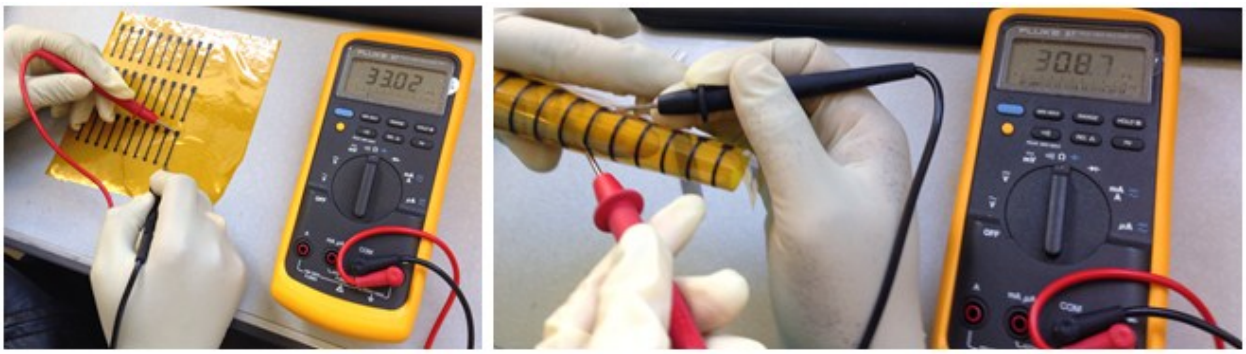

Figure S3: Mechanical bending test of a representative array of graphene electrodes printed on a polyimide sheet with 60 printing passes and a subsequent laser annealing with 40 mJ cm^{-2} energy density. The resistances in both the straight and bent states are almost identical with no apparent physical cracking of the printed graphene. The results show stable electrical conductivity even after multiple bending tests (i.e., 100 bending cycles), indicating the potential suitability of these printed graphene electrodes in a wide variety of applications were flexibility is paramount.

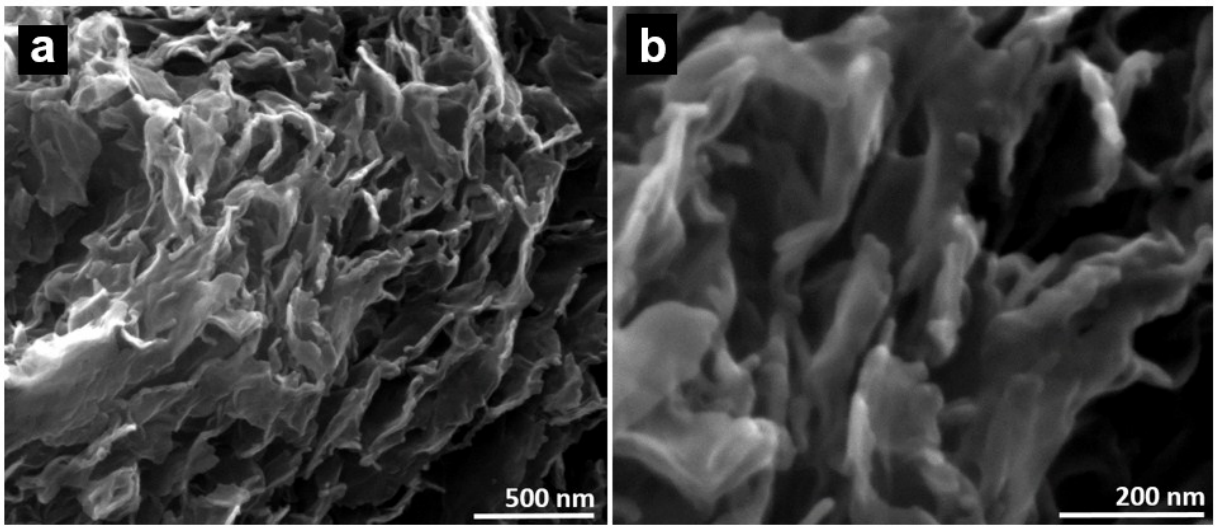

Figure S4: High resolution field effect scanning electron micrographs (FESEM) images of inkjet printed graphene on a polyimide substrate (same region with 2 different magnifications are shown). The graphene electrode was printed with 60 print passes and laser annealed with a power density of 85 mJ cm^{-2}. Vertical arrays of petal-like graphene with widths of 20 nm to 50 nm are visible.

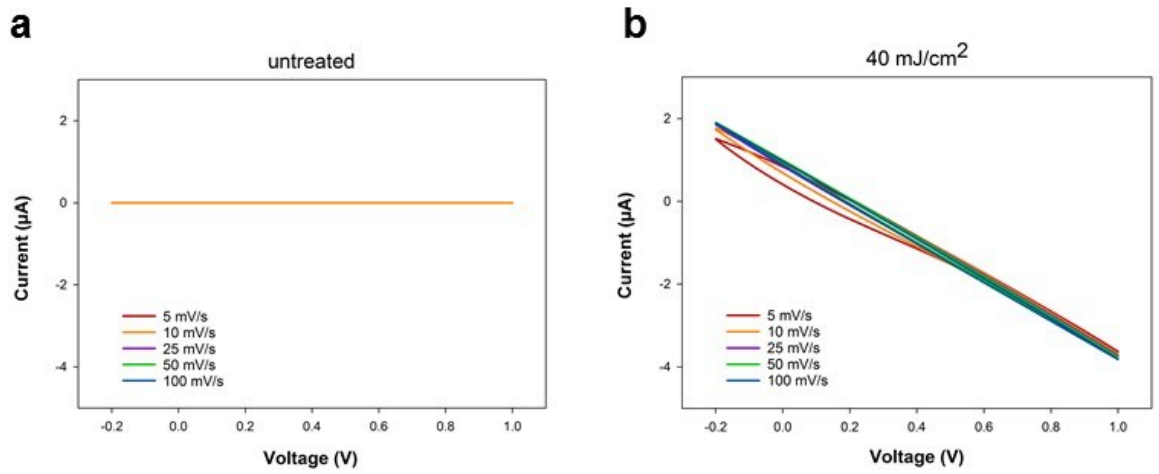

Figure S5: Cyclic voltammograms (CVs) of the inkjet printed graphene electrodes (**a**) without laser annealing, and (**b**) with laser annealing at a laser power density of 40 mJ cm^{-2}. The unannealed electrode (**a**) displays no change in the current with the sweeping of electrode voltage—indicating that unnannealed printed graphene is too resistive for electrochemical sensing. The laser annealed printed graphene electrode (**b**) displayed a very broad and relatively small redox peak at the lowest scan rate (5 mV/ sec). This CV indicates that even at low power densities, the laser annealing process can begin to transform the printed graphene into an electroactive surface.

Table S1: Comparison table of photon-based annealing techniques and the presented laser annealing technique for graphene-based surfaces.

	Continuous/ Pulsed photon	Wavelength exposure	Energy density	Power	Supplementary Reference #
Reduced graphene oxide	Continuous Infrared Laser (in DVD drive)	788 nm	-	5 mW	S1
Reduced graphene oxide	X-660 Laser Cutter platform (CO_2 laser)	10.6 μm	-	2.4 W	S2
Reduced graphene oxide	Continuous Wave Laser	532 nm	-	500 mW	S3
Inkjet-printed Graphene	Xenon Sinteron 2000 (pulsed)	240-1500 nm broad	25 J/cm^2 maximum	25 kW maximum	S4
Reduced graphene oxide	Yb-doped Potassium Gadolinium Tungstate Laser (pulsed)	1030 nm	50 mJ/cm^2	~ 3 E11 W	S6
Inkjet-printed reduced graphene oxide	Pulsed laser (Nd:Yag)	355 nm (3rd harmonic)	40 mJ/ cm^2	~ 2.7 MW	This work
Inkjet-printed reduced graphene oxide	Pulsed laser (Nd:Yag)	355 nm (3rd harmonic)	55 mJ/ cm^2	~ 4 MW	This work
Inkjet-printed reduced graphene oxide	Pulsed laser (Nd:Yag)	355 nm (3rd harmonic)	70 mJ/ cm^2	~ 5 MW	This work
Inkjet-printed reduced graphene oxide	Pulsed laser (Nd:Yag)	355 nm (3rd harmonic)	85 mJ/ cm^2	~ 5.7 MW	This work

3. References

[S1] El-Kady MF, Strong V, Dubin S, Kaner RB. *Science* 2012, **335**, 1326-1330.

[S2] Gao W. et al., *Nature Nanotechnology* 2011, **6**, 496-500.

[S3] Del SK. et al., *2D Materials* 2015, **2**, 011003.

[S4] Secor EB, Ahn BY, Gao TZ, Lewis JA, Hersam MC. *Adv Mater* 2015, **27**, 6683-6688.

[S5] A. Stukowski, *Modelling Simul. Mater. Sci. Eng.* 2010, **18**, 015012.

[S6] Viskadouros, G. et al., *Appl. Phys. Lett.* 2014, **105**, 203104.